PAPER

Check for updates

Waterborne superamphiphobic coatings with network structure for enhancing mechanical durability†

Wancheng Gu, Wei Wang, Xuan Jiao, Weilin Deng, Yage Xia, Xinquan Yu and Youfa Zhang 🆔 *

Superamphiphobic coatings may significantly change the wettability of a substrate, and so are attractive for applications in aero/marine engineering, biotechnology, and heat transfer. However, the coatings are caught in a double bind when their durability is considered, as they are vulnerable to mechanical abrasion. Meanwhile, the wide use of organic solvents for preparing the coatings generates environmental pollution. Here, we present a waterborne superamphiphobic coating through one-step spraying that repels a wide range of liquids. By tailoring the repellence of the nano-silica to waterborne resin, a network structure is constructed to protect the embedded nano-silica from damage. Thus, the coatings are durable against 725 cycles of friction tester abrasion under a load of 250 g, showing a significant improvement in the mechanical durability by 3–25 times. Moreover, our coating also shows excellent comprehensive durability, including resistance to oil-flow erosion, falling sand impact, chemical attack, thermal treatment, *etc.* This strategy can be introduced to various waterborne resins, demonstrating its universality, and may offer a new insight to design sustainable superamphiphobic coatings for long-term practical applications.

1. Introduction

Superamphiphobic coatings with the ability to repel liquids are of interest for fundamental research and practical applications in anti-fouling,[1–4] petrochemical engineering,[5–7] corrosion protection,[8,9] and heat transfer.[10–13] Characterizing with rough textures and low-surface-energy chemistry, these coatings enable a liquid drop on their surface to bead up and roll off readily.[14–19] Truly harnessing these preferred functions also calls for simultaneously preserving their mechanical durability; however, displaying such two features appears mutually exclusive.[20,21] This is because the liquid repellence requires a minimized interfacial contact area which typically takes advantage of trapping air pockets within refined structures, but makes a trade-off in mechanical durability, especially under abrasion conditions.[22,23] Meanwhile, the exposure of the underlying layer by abrasion may change the chemistry property of the surface, for example-the wettability, thereby leading to the adhesion of liquids to the surface.[24,25]

Diverse strategies have been developed to enhance the robustness of superamphiphobic surfaces. For example,

Jiangsu Key Laboratory of Advanced Metallic Materials, School of Materials Science and Engineering, Southeast University, Nanjing, 211189, PR China. E-mail: yfzhang@seu.edu.cn

† Electronic supplementary information (ESI) available. See https://doi.org/10.1039/d2ra02853k

adhesives, such as organic polymer or aluminum dihydrogen phosphate, can be introduced to improve the adhesion between the functionalized nanoparticle coating and the substrate.[26–28] However, the coatings lose their performance once the upper layer is abraded off, thereby leading to a moderate enhancement in durability. Alternatively, the strategy of the self-similar structure can achieve durability by sacrificing the upper layers,[29–31] which in turn compromises the lipophobicity. Currently, constructing a rigid armour can bear the mechanical load,[24,32–34] but poses a strict requirement on the specific substrate and advanced microfabrication technologies, which are low-throughput, time-consuming, and cost-ineffective. Besides, the preparation of most superamphiphobic surfaces depends on organic solvents to dissolve low-surface-energy substances,[30,35] which leads to environmental pollution. Although water is a green and safe choice as the solvent,[36] the incompatibility between the water and low-surface-energy substances impedes the preparation of waterborne superamphiphobic coatings. Consequently, most efforts have been focused on the preparation of the waterborne superamphiphobic coatings,[37–39] but rarely on the breakthrough in the durability. To date, it remains challenging to fabricate coatings while achieving both superamphiphobicity and durability by simple fabrication processes, especially for waterborne coatings.[40]

Here, water and waterborne resins are selected to prepare the superamphiphobic coatings. Although the repellence of the fluorinated nano-silica to waterborne resin was regarded as the
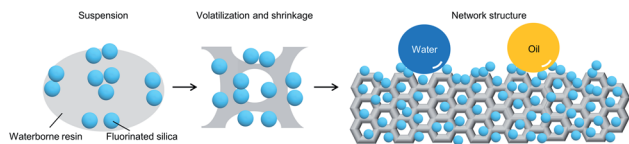
Fig. 1 Schematic illustration of network coating formation.

barrier to preparing waterborne superamphiphobic coatings, we utilize and control this property to the optimized one to promote the shrinkage of waterborne resin (Fig. 1). Then, the frame unit forms with cavities. After layer-by-layer spraying, the network structure is constructed with the embedment of fluorinated nano-silica. On the one hand, the embedded fluorinated nano-silica provides superamphiphobicity. On the other hand, the network structure can bear the external load to protect the embedded nano-silica, which promises the mechanical and environmental durability of superamphiphobic coatings. The new design principle for waterborne superamphiphobic coatings features the following advantages: (1) the coatings can be prepared by various waterborne resins in a facile and sustainable manner. (2) The coatings repel various liquids. (3) The coatings show a significant improvement in mechanical durability by 3–25 times and can withstand comprehensive harsh conditions.

2. Experimental section

2.1 Materials

Deionized water, nano-silica (average size: 13 nm), and commercial waterborne resins, including fluorocarbon resin (FEVE), epoxy, polyurethane, and acrylic resin, were all purchased from Wanqing Co. Ltd (China). Ammonia hydroxide (28 wt%) and $1H,1H,2H,2H$-perfluoro-decyltrichlorosilane (FDTS) were supplied by Aladdin Co. Ltd (China). Fluoro-carbon surfactant (Capstone FS-61) was purchased from DuPont Co. Ltd (USA).

2.2 Fabrication of network coating

The superamphiphobic nano-silica was prepared based on our previous work.[41] To prepare the waterborne coating, the ethanol solvent was replaced by water. 0.36 g of nano-silica was dispersed in the solution containing 90 mL of deionized water, 0.5 g of fluorocarbon surfactant, and 4 mL of ammonia hydroxide. Followed by mechanical stirring for 5 min, 0.35 mL of FDTS was added into the suspension drop by drop. After reaction for 12 h, the superamphiphobic nano-silica suspension was obtained. Then, the dry nano-silica was obtained by freeze-drying. After heat treatment at different temperatures for 10 min, 2 g of the fluorinated nano-silica was mixed with 5 g of the waterborne FEVE resin in 15 mL of deionized water. Finally, the waterborne network coating could be prepared through one-step spraying after heat treatment at different temperatures (*i.e.*, 180 °C, 200 °C, and 220 °C) for an hour. It is worth noting that the heat treatment of network coatings is the final treatment in the coating preparation, which is distinct from the heat treatment of the fluorinated nano-silica for tailoring its

wettability. For fabrication of the film and bulk, the aforementioned coating suspension was poured into a mould. After being fully cured for 48 h at room temperature and heat treatment at 180 °C for an hour, the film and bulk were obtained followed by demoulding.

For comparison, the layered coating was prepared by two-step spraying as reported in the conventional strategy.[26] The waterborne resin was first coated on the substrate as the adhesive. Then, the superamphiphobic nano-silica suspension was sprayed onto the semi-curing waterborne resin. Finally, the layered superamphiphobic coating was obtained by heating at 180 °C for an hour.

2.3 Characterization

Scanning electron microscopy (SEM, Nova Nano SEM450, FEI, USA) with an energy dispersive spectrometer (EDS), transmission electron microscopy (TEM, Talos F200X, Thermo Fisher Scientific, USA), and atomic force microscopy (AFM, Dimension ICON, Bruker, Germany) were used to observe the morphologies and structures of samples. The chemical composition was analyzed by X-ray photoelectron spectroscopy (XPS, Nexsa, Thermo Fisher Scientific, USA) and Fourier transform infrared spectra (FTIR, Nicolet IS-10, Nicolet, USA). Thermogravimetric (TG) measurement was conducted *via* a STA449-F3 Setsys Evolution (Netzsch, Germany) using a dynamic heating rate of 10 °C min^{-1}. The thickness and surface roughness of the coatings were measured by a surface profiler (D-100, KLA-Tencor, USA). The pore distributions and porosity were measured *via* a fully automatic surface area and porosity analyzer (ASAP 2460, Micromeritics, USA) by the Brunauer–Emmett–Teller (BET) method and mercury intrusion porosimetry (MIP, AutoPore Iv 9510, Micromeritics, USA). The static contact angles of liquids with 5 μL and roll-off angles of liquids with 10 μL were measured by a contact angle meter (OCA 15Pro, Dataphysics, Germany). Each sample was measured at five different positions.

2.4 Durability tests

The abrasion tests were respectively carried out using a friction tester (Biuged Laboratory Instruments Co. Ltd., China) and a Taber abrasion tester (TABER® INDUSTRIES, USA) according to ASTM D4060 standard. For friction tester abrasion (inset in Fig. 4b), the coatings on the glass substrates (the following samples were the same otherwise specially noted) were repeatedly abraded by a rubber under a 250 g load. Each back and forth movement of the rubber was counted as one abrasion cycle. The olive-oil stirring test was performed to evaluate the resistance to the erosion of oil flow. For this test, the sample was fixed in a beaker with the coating surface immersed in olive oil. The oil was stirred by a mechanical agitator at a speed of 2000 rpm (*i.e.*, ~15 m s^{-1} of linear speed). Sandy water stirring was performed for mimicking ship movement in the water with sand particles. The test was similar to the olive oil, except replacing olive oil with sandy water (sand content: 4 g L^{-1}). The resistance to mechanical impact was evaluated by the sand impact test. During the test, the sand fell at a rate of 40 g min^{-1}

from a height of 30 cm and impacted the coating surface which was tilted at 45°. The chemical stability was tested by directly immersing the coatings into chemical solutions, including 3.5 wt% NaCl solution, HCl solution (pH: 1–5), and NaOH solution (pH: 9–13). The thermal stability was tested by placing the coating in the liquid nitrogen (-196 °C), refrigerator (-30 to 0 °C), and oven (100–350 °C), respectively. For long-term thermal stability, we kept the sample on a heating stage at a temperature of 250 °C.

3 Results and discussion

3.1 Design of network coatings

We first tailored the wettability of fluorinated nano-silica to obtain the optimized repellence to waterborne resin (Fig. 2a). The fluorinated nano-silica turned hydrophilic due to the fluorocarbon surfactant (determined by the hydrophilic carboxyl groups), which was used to help water dissolve low-surface-energy substances (Fig. S1a†). This altered surface chemistry, which has been widely regarded as the failure in super-amphiphobicity, was investigated and then utilized to tailor the wettability of fluorinated nano-silica by controlling the decomposition of fluorocarbon surfactant (Fig. S1b†). Thus, the fluorinated nano-silica showed totally different wettability after heat treatment at different temperatures (Fig. S1c†).

The fluorinated nano-silica with a water contact angle of $\sim125°$ (*i.e.*, treated at 160 °C) repelled the waterborne FEVE resin and promoted its shrinkage, which is therefore the reasonable choice (Fig. 2b). The shrunken waterborne resin served as the skeleton to surround the fluorinated nano-silica and gradually constructed the network structure by layer-by-layer crosslinking, which was evidenced by the increasing roughness (Fig. S2†). Finally, the network structure formed with a stable roughness after heat treatment at 180 °C (Fig. 2c). Amounts of cavities with a diameter of 1–15 µm were uniformly distributed on the coating, and several small cavities were contained within the large cavities, showing an interconnected

frame, which seemed like a network. Note that, the continuous interconnected frame would be broken if further increasing the coating treatment temperature, thereby leading to the crack formation on the network structure (Fig. S3†). Moreover, it can be observed that the fluorinated nano-silica was embedded in the network structure. Due to the repellence, the fluorinated nano-silica avoided the excessive package by waterborne resin, thereby contributing to the roughness. However, it was impossible for constructing such a structure by using the fluorinated nano-silica with either insufficient or extreme repellence (Fig. S4†). For example, the fluorinated nano-silica treated at 100 °C possessed a water contact angle of $\sim58°$, showing an affinity to waterborne resin. The resultant coating showed a smooth structure with a few cavities. Conversely, the fluorinated nano-silica treated at 180 °C achieved super-amphiphobicity, meaning the excessive repellence to waterborne resin. The incompatibility led to the difficulty in mixing them. Thus, the coating showed a loose structure without the continuously interconnected bridges (*i.e.*, network structure). For comparison, the layered coating was prepared according to the conventional strategy (Fig. S5a†). The layered coating exhibited a relatively smooth structure (Fig. S5b†). Such a difference is evidenced by the porosity analyses, that the network coating possessed much more cavities than the layered coating, especially the micro-scale ones (Fig. S5c and d†). Note that, the cavities below 10 nm were formed by the stack of nano-silica.

Fig. 2d and S6a† show the surface chemistry of the network coating. The corresponding distributions of F and Si elements demonstrated the successful graft of FDTS on nano-silica, which provides low surface energy. Besides, the black regions in the maps referring to the cavities can also be observed. The FTIR spectra further verified the successful graft, that the peak intensity of –OH groups became weaker and a new peak of $-CF_2-$ groups emerged after nano-silica fluorination (Fig. S6b†). In addition, the peak of C=O groups (corresponding to the hydrophilic carboxyl groups as evidenced in Fig. S1a†) disappeared on the fluorinated silica after heat treatment at 180 °C, thereby removing the influence of the fluorocarbon surfactant on the superamphiphobicity. The entire coating was covered by $-CF_x$ groups with low surface energy.

Under the synergistic contribution of rough texture and low surface energy, the network coating, which was thicker than 45 µm, was super-repellent (*i.e.*, contact angle >150° and roll-off angle <10°) to a wide range of liquids, even the decane with a low surface tension of 23.8 mN m^{-1} (Fig. 2e, S7 and Table S1†). These drops of water, olive oil, hexadecane, ethanol solution (60 wt%), and decane sitting on the network coating were nearly spherical (inset in Fig. 2e). Moreover, our coating not only realized the superamphiphobicity in air, which allowed the falling decane droplet to bounce off the surface without adhesion, but also repelled the water in oil (Fig. S8†). Note that, due to the sufficient temperature of 180 °C to totally remove the fluorocarbon surfactant, the network coatings treated at higher temperatures showed a similar superamphiphobicity to that treated at 180 °C, despite crack formation on their network structure (Fig. S9†). Significantly, the reported strategies of the
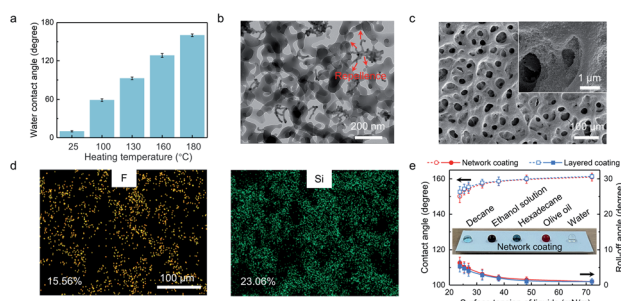

Fig. 2 Design of network coatings. (a) Wettability control of the fluorinated nano-silica by heat treatment at different temperatures. (b) TEM image showing the shrinkage of the waterborne resin driven by the fluorinated nano-silica. (c) Surface morphology of the network coating. The inset of the SEM image shows the embedment of fluorinated nano-silica in the network structure. (d) Element maps of F and Si of the network coating. (e) The contact angles and roll-off angles of liquids with various surface tensions. The inset of the optical photograph shows the repellence of the network coating to various liquids.

self-similar structure were achieved by mixing super-amphiphobic particles and adhesive/matrix. It leads to the excessive package of superamphiphobic particles by adhesive/matrix, which sacrifices the oleophobicity. However, our coating utilizes the controlled repellence of fluorinated nano-silica to waterborne resin, thereby mitigating the challenge and exhibiting a similar superamphiphobicity to the layered coating, whose fluorinated nano-silica was sprayed separately from the adhesive.

The new design concept of tailoring the repellence of fluorinated nano-silica also endowed our coating with universality. Our strategy could be introduced to various waterborne resins, whether oleophilic or oleophobic, and flexible or rigid (Fig. 3a and Table S2†). For example, the network coating achieved superamphiphobicity even using the waterborne epoxy resin with a water contact angle of ∼34.7° and an olive-oil contact angle of ∼15.8°. As shown in Fig. 3b, the spherical droplets of ethanol solution (60 wt%) stood on various network coatings. However, most reported durable superamphiphobic coatings were prepared by the specific or optimized matrix/adhesive after amounts of experiments.[27,28,31] From an engineering perspective, our coating could be applied to the propeller with a complex shape and a size of 0.55 m, demonstrating the simple and large-scale fabrication (Fig. 3c). The coated propeller was endowed with the self-cleaning property. The dust on the coating surface was removed by the ethanol solution flow and left a clean surface as described in Fig. S10.† Moreover, the versatility was demonstrated by preparing the network coating onto various substrates, such as rigid, flexible, smooth, and porous substrates, proposing the potential in various applications (Fig. S11†). We also fabricated the network bulk and film for friendly use, which could be attached to the substrates when
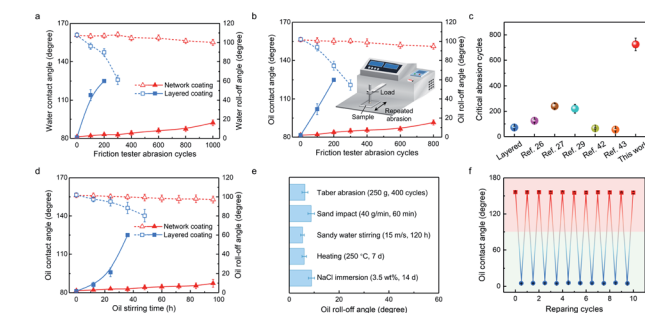

Fig. 4 Comprehensive durability of network coatings. (a and b) Water and olive-oil repellence of different coatings after friction tester abrasion. The inset of the schematic illustration shows the friction tester. (c) Comparison of the abrasion resistance of the network coating with that of the existing reports. (d) Olive-oil repellence of different coatings after oil stirring. (e) Comprehensive durability of the network coating. (f) The repairable property of the network coating.

required (Fig. 3d and S12†). The spherical droplets of ethanol solution stood on the upper and inner surface of the bulk, showing the all-dimensional superamphiphobicity. Besides, the network bulk and film with excellent flexibility could tolerate more than 100 cycles of bending without deformation.

3.2 Comprehensive durability

The durability of superamphiphobic coatings is crucial to practical applications. For example, repeated abrasion is common in daily life. Here, we first performed the friction tester abrasion under a load of 250 g. Consistent with our prediction, the network coating using both 180 °C heat treatment and fluorinated nano-silica treated at 160 °C showed the best abrasion resistance, which was used to examine the durability (Fig. S13†). As shown in Fig. 4a and b, our coating with a thickness of ∼80 μm exhibited a stable superamphiphobicity during the abrasion. The contact angles and roll-off angles of water and olive oil were still greater than 150° and less than 10°, respectively, even after 600 cycles of abrasion. Further increasing abrasion to 1000 cycles, water droplets can still easily roll off. In sharp contrast, the layered coating with the thickness of ∼100 μm showed a much faster deterioration of superamphiphobicity than the network coating and effortlessly lost the superamphiphobicity within 100 cycles of abrasion, thereby leading to the liquid adhesion. It is well known that coating durability relates to the coating thickness. We then determined the critical abrasion cycles—that is, the maximum number of abrasion cycles that the coating could withstand without a loss of performance, and showed the index of the network coatings with different thicknesses (Fig. S14†). The anti-abrasion capacity was enhanced with the thickness increment. From an engineering perspective, the relatively thin coating with a thickness of ∼80 μm was a reasonable choice, which achieved both satisfactory superamphiphobicity and durability. Therefore, we compared this index with various reported durable coatings,[26,27,29,42,43] whose minimum thickness was ∼100 μm (Fig. 4c). The critical abrasion cycles of our coating reached 725, which was 3–25 times higher than that of the reported coatings,
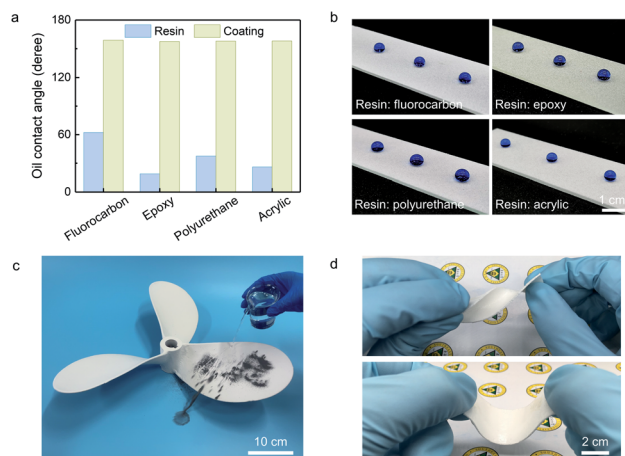

Fig. 3 Universality of network coatings. (a) The contact angles of olive oil on various waterborne resins and the corresponding network coatings. The network coating achieves superamphiphobicity even using the waterborne resin with an olive-oil contact angle of ∼16°. (b) Optical photographs of network coatings prepared by various waterborne resins, including fluorocarbon, epoxy, polyurethane, and acrylic resin. (c) Optical photograph of the network coating on the propeller with the complex shape. (d) Optical photograph of the network film with excellent flexibility.

demonstrating a significant improvement in mechanical durability. Note that, such an improvement effect was also applicable to other kinds of waterborne resins, meaning that the universality of our strategy covered both superamphiphobicity and mechanical stability (Fig. S15†).

We also performed oil stirring tests to demonstrate the durability of our coatings against soft mechanical damage. As shown in Fig. 4d, the network coating could tolerate the erosion of olive-oil flow for 96 h, which was 8 times longer than the layered coating. More comprehensive durability tests were conducted to simulate various environments in practical applications, including Taber abrasion for mechanical abrasion (400 cycles under a 250 g load), the sand impact for mechanical impact (40 g min^{-1} for 60 min), the sandy water stirring for flow erosion (15 m s^{-1} for 120 h), the chemical attack (immersion in 3.5 wt% NaCl solution for 14 days) and the heat treatment (250 °C for 7 days) (Fig. 4e). In addition, we also carried out the chemical attack tests induced by various corrosive solutions (pH value of 1–13 for 48 h) and the thermal stability tests at temperatures ranging from −196 to 350 °C for 2 h (Fig. S16†). Our coatings could withstand all these extremely harsh conditions, maintaining the roll-off angles of olive oil less than 10°. Significantly, the excellent durability of the network coatings could be realized not only on the glass substrate but also on the steel substrate (Fig. S17†). Note that, coating adhesion is also an important factor for durability. The cross-hatch test was performed on the coating followed by tape peeling (ASTM D3359-17 standard). Almost no removal of coating can be observed, demonstrating the strong adhesion of the network coating (Fig. S18†).

Moreover, our coating was endowed with the repairable property, which further improved the reliability for practical applications. As shown in Fig. 4f, the network coating turned oleophilic after oxygen plasma treatment. Then the super-amphiphobicity was regenerated by sandpaper abrasion. The procedure of oxygen plasma treatment and abrasion was counted as one cycle. Our coating could be repaired over 10 cycles, without deterioration of superamphiphobicity.

3.3 Mechanical stability mechanism

The superior durability of our coating is attributed to the network structure. As shown in Fig. 5a, during abrasion, the network structure tolerates the external force and prevents the embedded nano-silica from removal. Such protection could be evidenced by the surface morphology of the abraded network coating (Fig. 5b). Several cavities (5–75 μm) could be observed, which are much smaller than the abradants. Although the skeletons (superficial structure) underwent the severe damage, the nano-silica remained intact within the cavities to provide superamphiphobicity. The AFM image also shows the rough structure within the cavities, further demonstrating the protection (Fig. 5c). However, the adhesive of the layered coating only plays a role in binding the nano-silica. Without the structure for protection, the nano-silica is vulnerable to mechanical abrasion (Fig. 5d). Therefore, the layered coating turned smooth after abrasion, and the nano-silica was almost completely removed, leading to the absence of roughness and
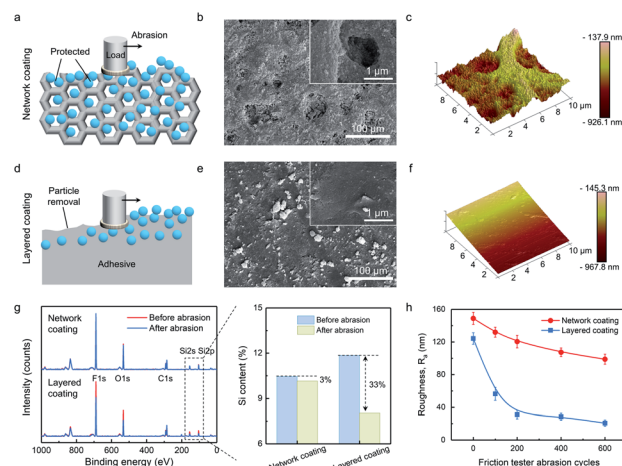

Fig. 5 Mechanical stability mechanism. (a) Schematic illustration showing the protection of the network structure for embedded nano-silica. (b and c) SEM and 3D-view AFM images of the network coating after abrasion. (d) Schematic illustration of the easy removal of fluorinated nano-silica on the layered coating. (e and f) SEM and 3D-view AFM images of the layered coating after abrasion. (g) Wide-scan XPS spectra of the surface elements of the network coating and layered coating before and after abrasion. (h) The change in coating roughness along with abrasion. All coatings were abraded by 600 cycles of friction tester abrasion.

low-surface-energy chemistry (Fig. 5e and f). We also used a micro-scratching test to visualize the behavior of the coating surface under scratching (Fig. S19a†). With a tip size of 5 μm, the indenter applied a 400 MPa load to the coating surface, which is much more severe than daily abrasion. Even so, the network structure tolerated the major stress and kept the nano-silica on the surface (Fig. S19b†). In contrast, the upper layer of the layered coating was entirely scratched off, leaving the adhesive layer alone (Fig. S19c†).

Such differences can be demonstrated from both aspects of chemical component and roughness. For the network coating, the reduction of Si content, which represents fluorinated nano-silica, was only 3% even after 600 cycles of abrasion (Fig. 5g). This is a negligible contribution to the degradation of super-amphiphobicity. However, the loss of nano-silica on the layered coating reached 33%, indicating 11 times higher than that on the network coating. Meanwhile, the roughness change of the network coating was also much slower than that of the layered coating (Fig. 5h). After 600 cycles of abrasion, the network coating still kept its roughness larger than 100 nm, indicating strong structural stability. The result posed a sharp contrast to that of the layered coating, whose roughness was rapidly reduced to only ∼30 nm within 200 cycles of abrasion. Together, these microscopic results demonstrate the notable resistance of network structure that significantly enhances mechanical durability.

4 Conclusions

In summary, we demonstrate a facile, scalable, and sustainable approach to creating waterborne superamphiphobic coatings.

By controlling the repellence of fluorinated nano-silica to waterborne resin, the coatings consist of the network structure for resisting damage and the embedded fluorinated nano-silica for repelling a wide range of liquids. Under the protection of network structure, the coatings preserve their super-amphiphobicity after 725 cycles of friction tester abrasion under a load of 250 g, boosting mechanical durability by 3–25 times, compared to those conventional coatings. Meanwhile, the coating demonstrates superior mechanical stability and long-term durability towards comprehensive tests under various harsh environments. Moreover, this strategy can be applied to various waterborne resins to improve the universality of superamphiphobic coatings. The findings provide a new design to strengthen the mechanical stability of waterborne super-amphiphobic coatings and show the wide application prospects in fuel transportation, anti-fouling, architecture, and other fields, especially for those that require durability under harsh conditions.

Author contributions

Wancheng Gu: methodology, investigation, writing – original draft. Wei Wang: methodology. Xuan Jiao: writing – review & editing. Weilin Deng: data curation. Yage Xia: resources. Xinquan Yu: supervision. Youfa Zhang: conceptualization, funding acquisition.

Conflicts of interest

There are no conflicts to declare.

Acknowledgements

Notes and references

1 J. Genzer and K. Efimenko, *Biofouling*, 2006, **22**, 339.
2 B. N. Sahoo, N. S. K. Gunda, S. Nanda, J. A. Kozinski and S. K. Mitra, *ACS Sustainable Chem. Eng.*, 2017, **5**, 6716.
3 J. Zhang, W. Wang, S. Zhou, H. Yang and C. Chen, *Prog. Org. Coat.*, 2019, **134**, 312.
4 Z. Zhang, D. Yu, X. Xu, H. Yang, I. Wyman, J. Wang and X. Wu, *Chem. Eng. Sci.*, 2021, **230**, 116182.
5 H. Han, J. S. Lee, H. Kim, S. Shin, J. Lee, J. Kim, X. Hou, S.-W. Cho, J. Seo and T. Lee, *ACS Nano*, 2018, **12**, 932.
6 C. R. Crick, J. A. Gibbins and I. P. Parkin, *J. Mater. Chem. A*, 2013, **1**, 5943.
7 J. Li, C. Xu, C. Guo, H. Tian, F. Zha and L. Guo, *J. Mater. Chem. A*, 2018, **6**, 223.
8 X. Zhao, J. Wei, B. Li, S. Li, N. Tian, L. Jing and J. Zhang, *J. Colloid Interface Sci.*, 2020, **575**, 140.
9 X. Zhang, F. Jiang, R. Chen, Y. Chen and J. Hu, *Corros. Sci.*, 2020, **173**, 108797.
10 K. Zhang, F. Liu, A. J. Williams, X. Qu, J. J. Feng and C. H. Chen, *Phys. Rev. Lett.*, 2015, **115**, 074502.
11 H. Vahabi, W. Wang, J. M. Mabry and A. K. Kota, *Sci. Adv.*, 2018, **4**, eaau3488.
12 K. L. Wilke, D. J. Preston, Z. Lu and E. N. Wang, *ACS Nano*, 2018, **12**, 11013.
13 X. Gong, X. Gao and L. Jiang, *Adv. Mater.*, 2017, **29**, 1703002.
14 T. L. Liu and C.-J. Kim, *Science*, 2014, **346**, 1096.
15 L. Zhang, A. G. Zhou, B. R. Sun, K. S. Chen and H. Z. Yu, *Nat. Commun.*, 2021, **12**, 982.
16 S. Pan, R. Guo, M. Bjornmalm, J. J. Richardson, L. Li, C. Peng, N. Bertleff-Zieschang, W. Xu, J. Jiang and F. Caruso, *Nat. Mater.*, 2018, **17**, 1040.
17 H. Liu, Y. Wang, J. Huang, Z. Chen, G. Chen and Y. Lai, *Adv. Funct. Mater.*, 2018, **28**, 1707415.
18 S. Martin and B. Bhushan, *J. Colloid Interface Sci.*, 2017, **488**, 118.
19 Z. Chen, Y. Hu, X. He, Y. Xu, X. Liu, Y. Zhou, L. Hao and Y. Ruan, *RSC Adv.*, 2022, **12**, 297.
20 A. Dhyani, J. Wang, A. K. Halvey, B. Macdonald, G. Mehta and A. Tuteja, *Science*, 2021, **373**, 294.
21 T. S. Wong, S. H. Kang, S. K. Y. Tang, E. J. Smythe, B. D. Hatton, A. Grinthal and J. Aizenberg, *Nature*, 2011, **477**, 443.
22 M. Li, W. Huang, C. Ren, Q. Wu, S. Wang and J. Huang, *RSC Adv.*, 2022, **12**, 11517.
23 X. Tian, T. Verho and R. H. A. Ras, *Science*, 2016, **352**, 142.
24 D. Wang, Q. Sun, M. J. Hokkanen, C. Zhang, F. Lin, Q. Liu, S. Zhu, T. Zhou, Q. Chang, B. He, Q. Zhou, L. Chen, Z. Wang, R. H. A. Ras and X. Deng, *Nature*, 2020, **582**, 55.
25 A. Milionis, E. Loth and I. S. Bayer, *Adv. Colloid Interface Sci.*, 2016, **229**, 57.
26 Y. Lu, S. Sathasivam, J. Song, C. R. Crick, C. J. Carmalt and I. P. Parkin, *Science*, 2015, **347**, 1132.
27 M. Liu, Y. Hou, J. Li, L. Tie, Y. Peng and Z. Guo, *J. Mater. Chem. A*, 2017, **5**, 19297.
28 Z. Xiao, H. Zhu, S. Wang, W. Dai, W. Luo, X. Yu and Y. Zhang, *Adv. Mater. Interfaces*, 2020, **7**, 2000013.
29 Y. Zhang, L. Zhang, Z. Xiao, S. Wang and X. Yu, *Chem. Eng. J.*, 2019, **369**, 1.
30 C. Peng, Z. Chen and M. K. Tiwari, *Nat. Mater.*, 2018, **17**, 355.
31 K. Golovin, M. Boban, J. M. Mabry and A. Tuteja, *ACS Appl. Mater. Interfaces*, 2017, **9**, 11212.
32 V. Kondrashov and J. Rühe, *Langmuir*, 2014, **30**, 4342.
33 J. G. Kim, H. J. Choi, K. C. Park, R. E. Cohen, G. H. McKinley and G. Barbastathis, *Small*, 2014, **10**, 2487.
34 L. B. Boinovich, E. B. Modin, A. R. Sayfutdinova, K. A. Emelyanenko, A. L. Vasiliev and A. M. Emelyanenko, *ACS Nano*, 2017, **11**, 10113.
35 D. Zhi, Y. Lu, S. Sathasivam, I. P. Parkin and X. Zhang, *J. Mater. Chem. A*, 2017, **5**, 10622.
36 S. Jiang, A. Van Dyk, A. Maurice, J. Bohling, D. Fasano and S. Brownell, *Chem. Soc. Rev.*, 2017, **46**, 3792.
37 H. Zhou, H. Wang, H. Niu, Y. Zhao, Z. Xu and T. Lin, *Adv. Funct. Mater.*, 2017, **27**, 1604261.
38 J. E. Mates, R. Ibrahim, A. Vera, S. Guggenheim, J. Qin, D. Calewarts, D. E. Waldroup and C. M. Megaridis, *Green Chem.*, 2016, **18**, 2185.

39 K. Chen, S. Zhou, S. Yang and L. Wu, *Adv. Funct. Mater.*, 2015, **25**, 1035.

40 X. Wu, I. Wyman, G. Zhang, J. Lin, Z. Liu, Y. Wang and H. Hu, *Prog. Org. Coat.*, 2016, **90**, 463.

41 X. Jiao, M. Li, X. Yu, W. S. Y. Wong and Y. Zhang, *Chem. Eng. J.*, 2021, **420**, 127606.

42 S. Wang, X. Yu and Y. Zhang, *J. Mater. Chem. A*, 2017, **5**, 23489.

43 X. Deng, L. Mammen, H. J. Butt and D. Vollmer, *Science*, 2012, **335**, 67.